Supporting information

Nano-V_2O_5/Ti porous membrane electrode with enhanced electrochemical activity for the high-efficiency oxidation of cyclohexane

Yujun Zhang [a,b], Yubo Qi [a,b], Zhen Yin [a,c,], Hong Wang [a,b], Benqiao He [a,b], Xiaoping Liang [a,b], Jianxin Li [a,b,]*, Zhenhuan Li [a,b]*

[a] State Key Laboratory of Separation Membranes and Membrane Processes/National Center for International Joint Research on Separation Membranes, Tianjin Polytechnic University, Tianjin 300387, PR China

[b] School of Materials Science and Engineering, Tianjin Polytechnic University, Tianjin 300387, PR China

[c] School of Environmental and Chemical Engineering, Tianjin Polytechnic University, Tianjin 300387, PR China

*Corresponding author. TEL: +86-22-8395 5798; fax: +86 22 8395 5055

E-mail: yinzhen@tjpu.edu.cn (Dr. Z. Yin); jxli@tjpu.edu.cn (Dr. J. Li)

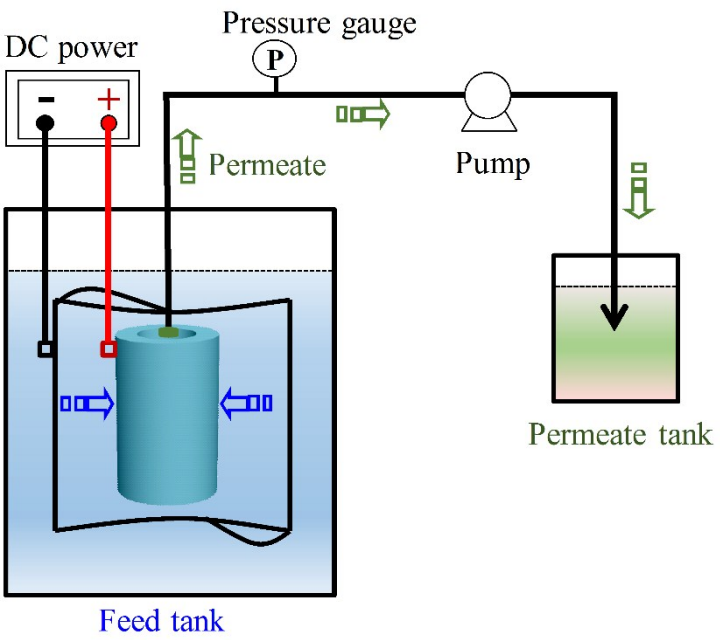

Fig. S1. Schematic diagram of the ECMR.

In the ECMR, a direct current (DC) (Maynuo M8811) continuously supplied the cleanest reagents – electrons. The V_2O_5/Ti membrane electrode as an anode transferred the electron between the electrode and reactants in the solution. The current circuit was completed with an auxiliary cathode of stainless steel, in which the distance of the two electrodes was 25 mm. The ECMR adopted a peristaltic pump to drive the reactants in the feed tank to the surface of V_2O_5/Ti membrane electrode and the products out the electrode to permeate tank. The CHA oxidation process is very temperature dependent and the stainless steel water bath was applied to regulate temperature. 5 g L^{-1} NaOH was used as electrolyte.

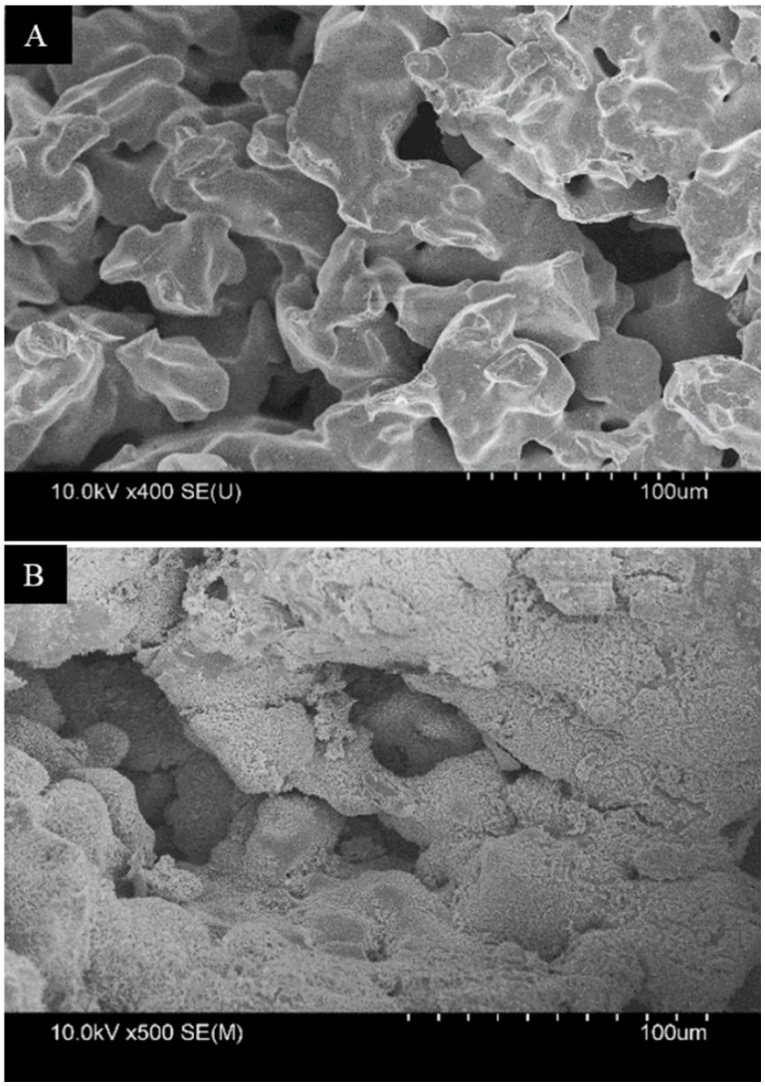

Fig. S2. FESEM images of Ti membrane without (A) and with (B) V_2O_5 NSs.

The images in Fig. S2 indicated V_2O_5 NSs were evenly distributed on the surface of the porous Ti membrane.

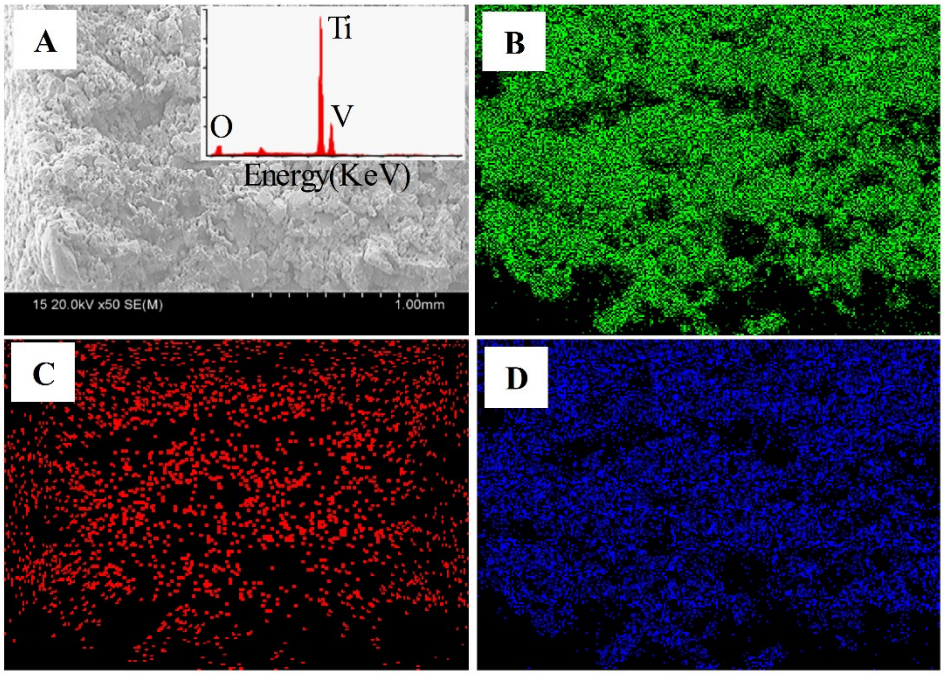

Fig. S3. FESEM images (A), EDS result inset in (A) and elements mapping of Ti (B), O (C), V (D) from V_2O_5 NSs/Ti electrode.

Fig. S3A showed the existence of V_2O_5 on the surface of the porous Ti membrane. The mapping (Fig. 3B-3D) indicated V_2O_5 catalysts were evenly distributed on the surface of porous Ti membrane. The mapping results were consistented with the FESEM image as shown in Fig. S2B.

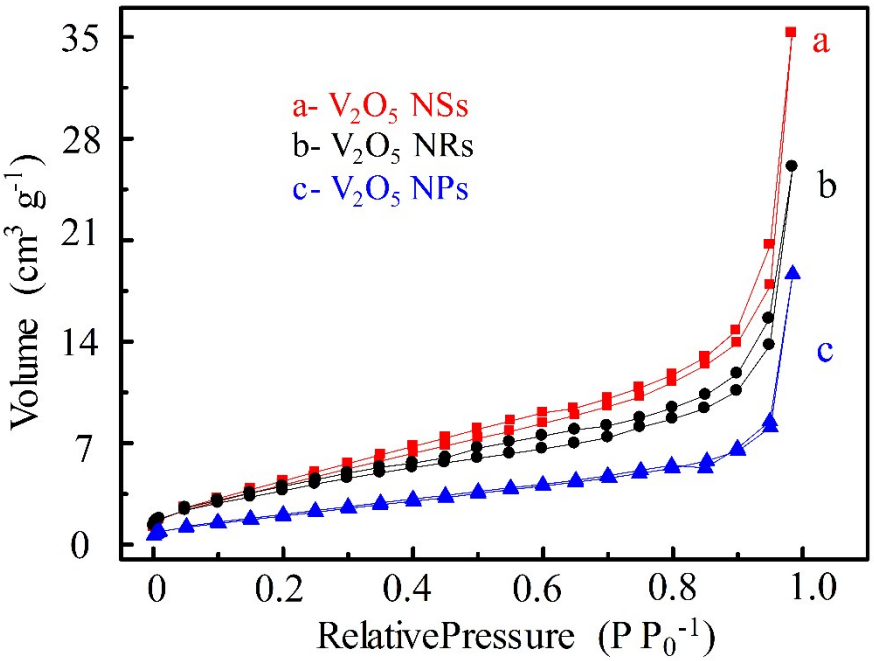

Fig. S4. N_2 sorption isotherms of V_2O_5 NRs, NSs, NPs.

As shown in Fig. S4, the specific surface areas of V_2O_5 NSs, NRs, NPs were calculated from the adsorption data using the Brunauer–Emmett–Teller (BET) method, and the values were 35.2, 28.8, 17.5 m^2 g^{-1}, respectively.

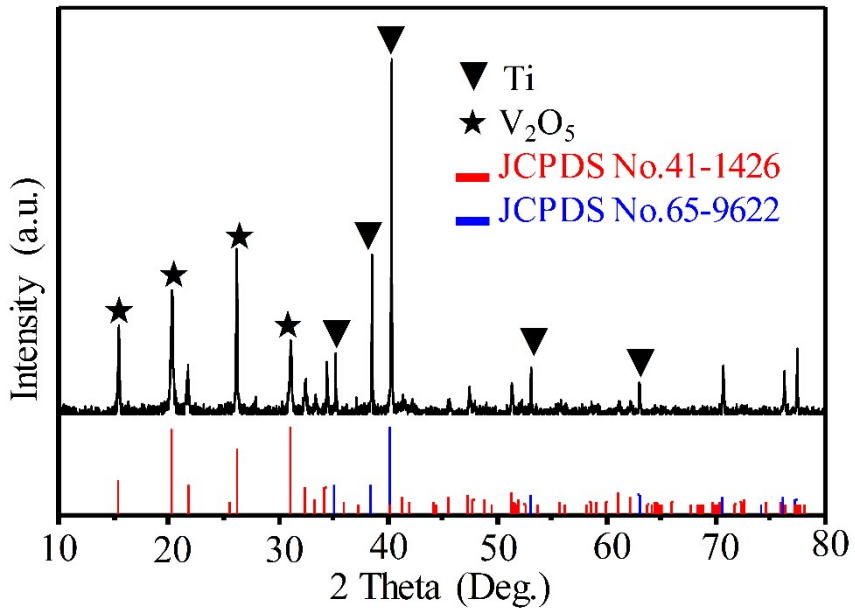

Fig. S5. XRD pattern of V_2O_5 NSs/Ti membrane electrode.

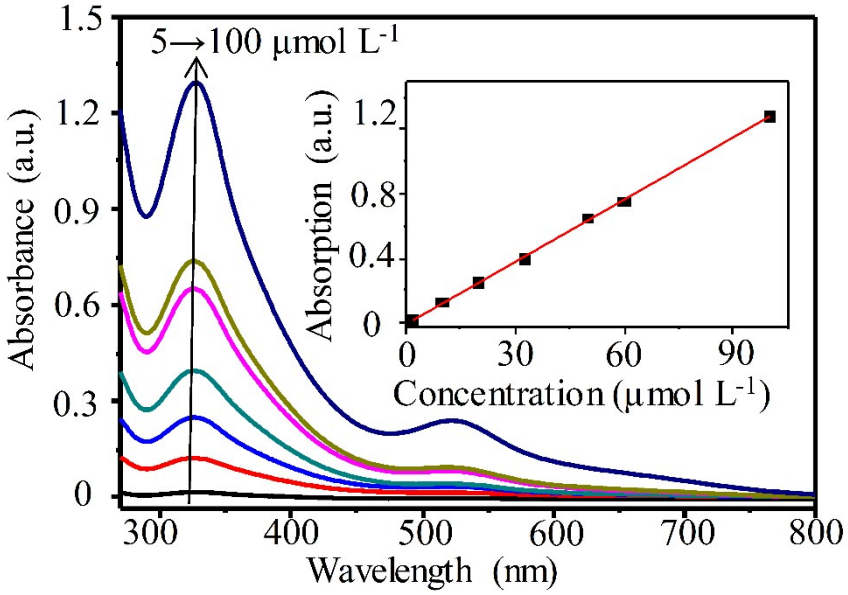

Fig. S6. UV-vis absorbance spectra at various concentrations of DPPH·. The inserted figure indicated the changes on the absorption of DPPH· with various concentrations at 328 nm.

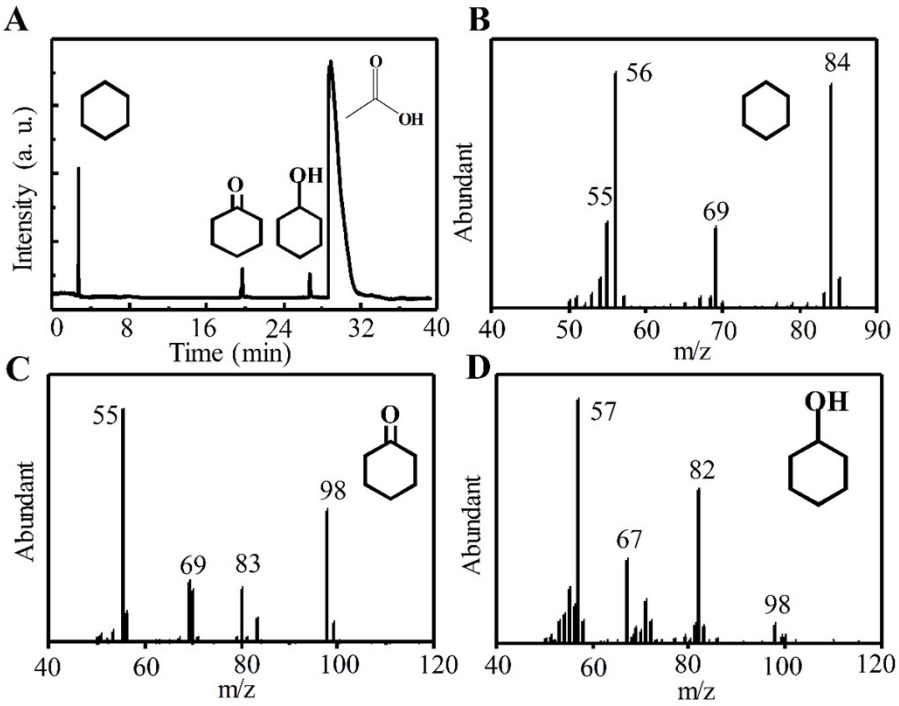

Fig. S7. GC-mass spectra of permeate: GC chromatogram (A), mass spectra of CHA (B), K (C), A (D).

The products were analyzed by mass spectra (Agilent 5973N) and gas chromatography (GC) (Agilent 7890A) with DB-FFAP capillary column and flame ionization detector (FID). As shown in Fig. S6, the retention time of A, K was 27.0 min, 19.7 min, respectively.

Table S1. A comparative study on the catalytic activities of different catalysts in cyclohexane oxidation.

Entry	Catalyst	Oxidant	Condition	Time	Conv. (%)	Select. (%)	Ref.
1	Graphene/C_3N_4	O_2	150 ^oC	4 h	14.0	K:98	(1)
2	Au Clusters/ Hydroxyapatite	O_2, TBHP	150 ^oC	4 h	14.9	KA:99	(2)
3	Au/CQDs	H_2O_2	Green light	48 h	63.8	KA:99	(3)
4	Tetrabutylammonium decatungstate	O_2	Solar simulator	6 h	Yield = 68		(4)
5	Polyoxometalate anions (POMs)	O_2	Visible light, 36-38 ^oC	12 h	26.5	KA:99.1	(5)
6	BiOI	O_2	Visible light, 37 ^oC	3 h	16.5	KA:99	(6)
7	V-substituted HPAs	N_2O	Visible light	12 h	26.2	KA:90.2	(7)
8	C_3N_4/Au	None	Visible light, 60 ^oC	24 h	10.54	K:100	(8)
9	V_2O_5 NSs/Ti	None	4.8 V, 30 ^oC	39.4 min	28.4	KA:99	This work

(1) X. H. Li, J. S. Chen, X. Wang, J. Sun and M. Antonietti, J. Am. Chem. Soc., 2011, 133, 8074-8077.

(2) Y. Liu, H. Tsunoyama, T. Akita, S. Xie and T. Tsukuda, ACS Catal., 2011, 1, 2-6.

(3) R. Liu, H. Huang, H. Li, Y. Liu, J. Zhong, Y. Li, S. Zhang and Z. Kang, ACS Catal., 2014, 4, 328-336.

(4) G. Laudadio, S. Govaerts, Y. Wang, D. Ravelli, H. F. Koolman, M. Fagnoni, S. W. Djuric and T. Noel, Angew. Chem. Int. Ed., 2018, 57, 4078-4082.

(5) S. Tang, J. She, Z. Fu, S. Zhang, Z. Tang, C. Zhang, Y. Liu, D. Yin and J. Li, Appl. Catal. B: Environ., 2017, 214, 89-99.

(6) A. Henríquez, H. D. Mansilla, A. M. Martínez-de la Cruz, J. Freer and D. Contreras, Appl. Catal. B: Environ., 2017, 206, 252-262.

(7) J. She, Z. Fu, J. Li, B. Zeng, S. Tang, W. Wu, H. Zhao, D. Yin and S. R. Kirk, Appl. Catal. B: Environ., 2016, 182, 392-404.

(8) J. Liu, Y. Yang, N. Liu, Y. Liu, H. Huang and Z. Kang, Green Chem., 2014, 16, 4559-4565.

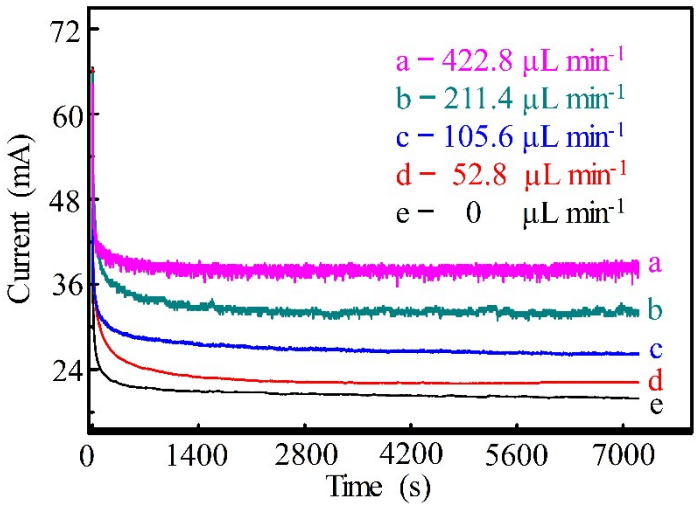

Fig. S8. Chronoamperometry plots of V_2O_5 NSs/Ti membrane electrode in ECMR with different permeate flow rate.

An interesting phenomenon can be seen from Fig. S7 that the currents obtained from the membrane electrode decreased rapidly, then tended to be a horizontal line, and finally reached a steady-state value. Notably, the steady-state values of current increased from 19.9 to 38.7 mA with the increase of permeate flow rate from 0 to 422.8 μL min^{-1}. It indicated that there existed an effect of enhanced mass transfer. That is to say, the enhanced mass transfer would promote the catalytic efficiency during ECRM operating.

Table S2. The current efficiencies (CE_T (%)) of ECMR with V_2O_5 NSs/Ti membrane electrode at different flow rate of solution.

Q (μL min^{-1})	52.8	105.6	211.4	422.8
CE_T (%)	17.6	23.4	34	49.6

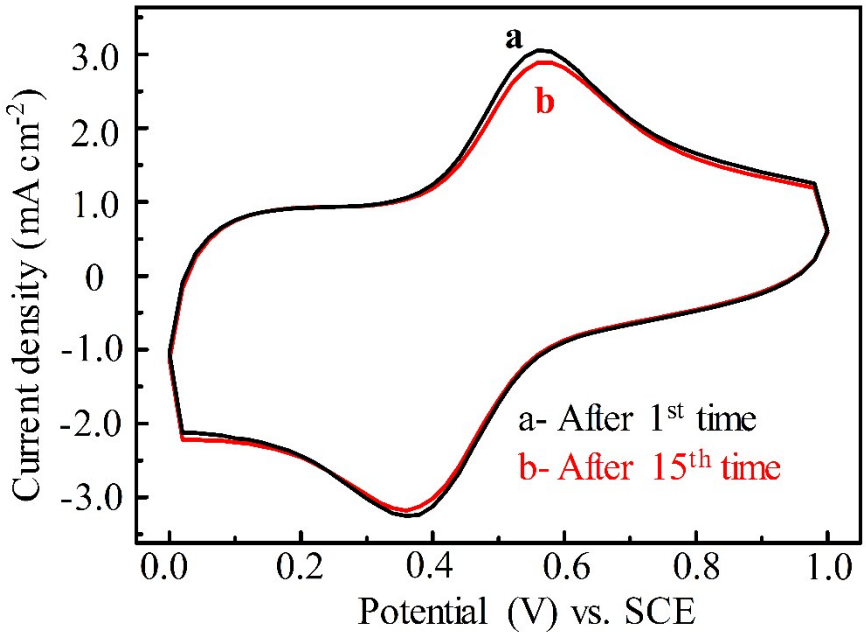

Fig. S9. CV curves of V_2O_5 NSs/Ti electrode after the 1st and 15th time of repeated use.

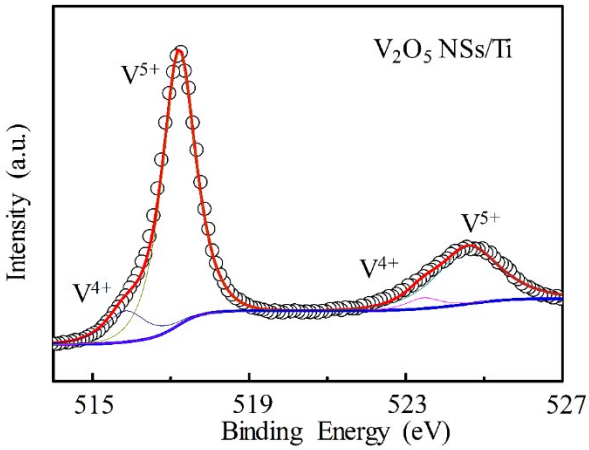

Fig. S10. XPS spectrum of the used V_2O_5 NSs/Ti.

As shown in Fig. S10, V^{4+} occupied up to approximate 10% on the used V_2O_5 NSs/Ti, which displayed that the ratio of V^{4+} kept relatively stable at 10% during the reaction.

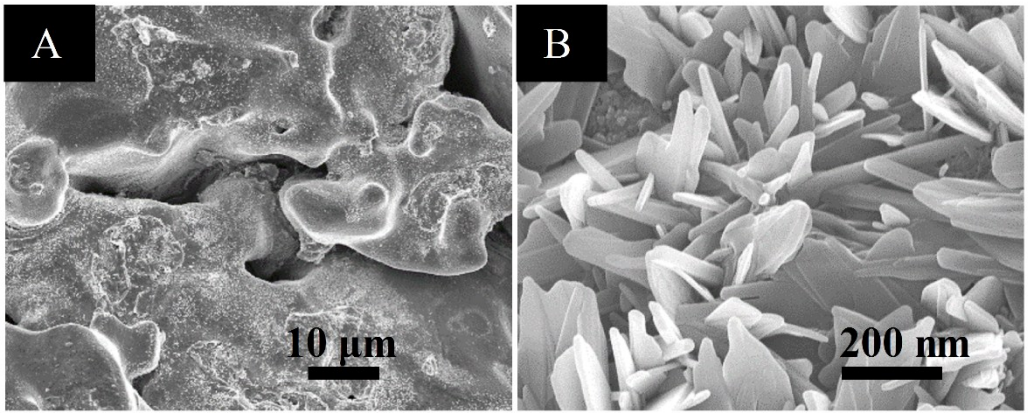

Fig. S11. FESEM images of the used V_2O_5 NSs/Ti.

After the reaction, the catalysts were still evenly distributed on the surface of the porous Ti membrane, and the nanosheets structure was no changed.

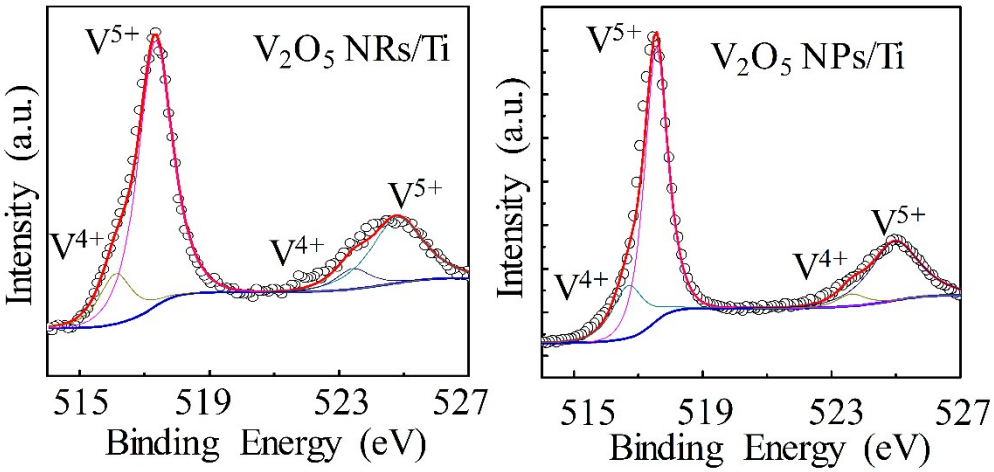

Fig. S12. XPS spectra of V_2O_5 NRs/Ti and V_2O_5 NPs/Ti electrode.

Fig. S9 showed the catalysts of vanadium oxide loading on Ti membrane contained various valence states, such as V^{5+}, V^{4+}. Moreover, the higher valence of V^{5+} was approximately 90% from V_2O_5 NRs/Ti and V_2O_5 NPs/Ti electrodes.

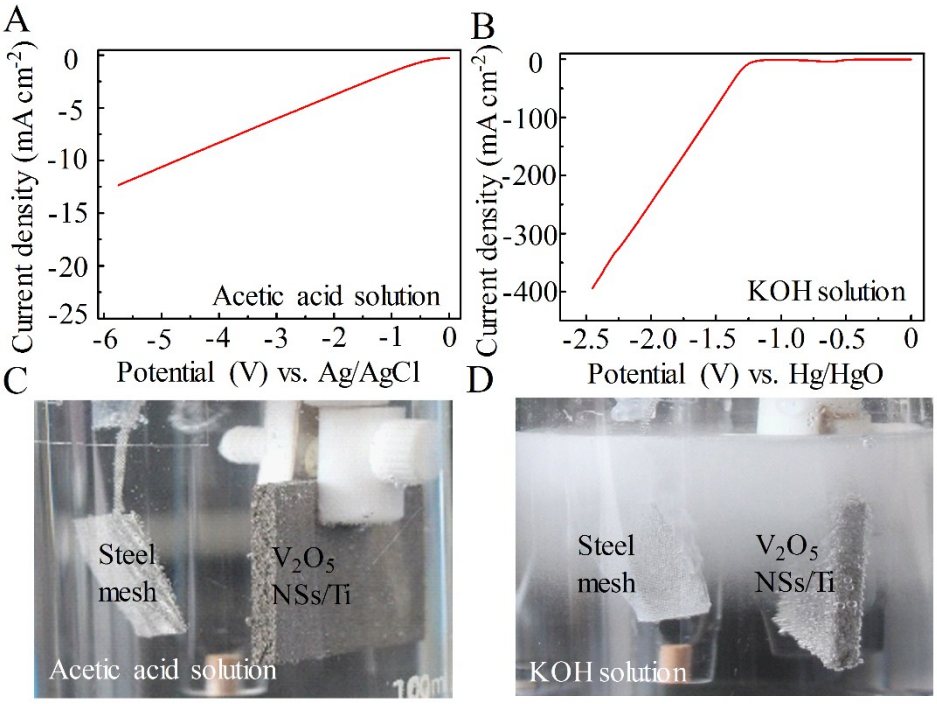

Fig. S13. Polarization curves, the pictures of H_2-evolution of steel mesh in acetic acid solution (A, C) and KOH solution (B, D), respectively.

The H_2-evolution reaction in the process of CHA oxidation was investigated. A three-electrode cell system was employed with steel mesh as working electrode, V_2O_5 NSs/Ti as the counter electrode, an Ag/AgCl (KCl, 3 mol L^{-1}) electrode as the reference electrode in acetic acid solution and a Hg/HgO electrode as the reference electrode in KOH solution. As shown in Fig. S10A and 10B, the current densities were 250 mA cm^{-2} (the steel mesh in KOH solution) and 3.78 mA cm^{-2} (the steel mesh in acetic acid solution) under the same potential of 2 V, respectively. That is to say, the activity of steel mesh in acetic acid solution was lower than that in KOH solution. Moreover, small amounts of bubbles were produced in acetic acid solution, but many bubbles are produced in KOH solution under 4.8 V as shown in Fig. S10C and 10D. It implied that

the electrochemical reaction with steel mesh in acetic acid solution had a quite lower activity for H_2-evolution and with a low safety risk. Certainly, H_2 generation will be consideration in the future investigated.